Chapter 23

Using Planar Phi29 pRNA Three-Way Junction to Control Size and Shape of RNA Nanoparticles for Biodistribution Profiling in Mice

Farzin Haque, Congcong Xu, Daniel L. Jasinski, Hui Li, and Peixuan Guo

Abstract

RNA is rapidly emerging as a versatile building block for nanoparticle assembly due to its simplicity in base pairing, while exhibiting diversity in function such as enzymatic activity similar to some proteins. Recent advances in RNA nanotechnology have generated significant interests in applying RNA nanoparticles for various applications in nanotechnology and nanomedicine. In particular, assessing the effect of size and shape on cell entry and intracellular trafficking as well as in vivo biodistribution of nanoparticles is challenging due to the lack of nanoparticles rich in structure while varying in size and shape. RNA nanotechnology exemplified by the packaging RNA (pRNA) of bacteriophage phi29 DNA packaging motor has provided a different prospect in nanoparticle designs. Of note, there is a robust three-way junction (3WJ) motif in pRNA which can serve as an adaptable scaffold to construct thermodynamically stable 2D planar and 3D globular RNA architectures with tunable shapes and sizes, and harboring various targeting, therapeutic, and imaging modules. This chapter focuses on the methods for constructing pRNA-3WJ based nanoparticles with controllable sizes and shapes, and assessment of their biodistribution profiles in cancer mouse models after systemic injection and ocular mouse models following subconjunctival injection.

Key words Nanobiotechnology, RNA nanoparticle, 3WJ, pRNA, Subcutaneous and orthotopic xenograft, Ocular delivery, Subconjunctival injection

1 Introduction

Nature has evolved smart building blocks for constructing sophisticated higher-ordered structures with unique functionalities. One of the burgeoning areas of nanobiotechnology is to exploit these biological building blocks for engineering nanosystems with de novo functionalities in order to probe and reprogram cells for therapeutic intervention. Lipid-based nanoparticles have been extensively

Authors "Farzin Haque" and "Congcong Xu" have contributed equally to this work.

Eckart Bindewald and Bruce A. Shapiro (eds.), *RNA Nanostructures: Methods and Protocols*, Methods in Molecular Biology, vol. 1632, DOI 10.1007/978-1-4939-7138-1_23, © Springer Science+Business Media LLC 2017

studied in the nanomedicine field due to their intrinsic structural simplicity and ease of encapsulating a variety of cargoes [1, 2]. However, they generally lack thermodynamic stability and often display off-target effects. Peptide and protein based scaffolds have propensity to aggregate, and lack scaffold addressability and structural fidelity, which limits their overall utility to generate programmable nanostructures [3]. Nucleic acids on the other hand are structurally highly programmable, and recent advances in nucleic acid chemistry have enabled the production of DNA and RNA nanoparticles with improved chemical and biological stability under physiological conditions [4, 5]. Rational design and assembly of DNA nanostructures was first conceived by Seeman in 1983 [6] and since then various applications of DNA nanostructures particularly in materials sciences have emerged [7, 8]. The principle is based on a simple set of construction rules relying on canonical Watson–-Crick interactions (A–T and G–C) to generate programmable DNA nanostructures. As an alternative to DNA, RNA has emerged as a more powerful building block for fabricating nanoparticles due to its diversity in structure and function, and high thermodynamic stability [5].

RNA nanotechnology refers to the study of nanoscale RNA architectures with its major frame composed mainly of RNA [5]. Scaffold, targeting ligands, therapeutic modules and regulators can be all composed of RNA nucleotides. Different from classical studies on RNA structure and function focused on intramolecular interactions and 2D/3D structures, current exploration of RNA in nanotechnology field pays close attention to intermolecular interactions and quaternary structures. RNA nanostructure formation is much more complex relying on both canonical and noncanonical (such as G–U) base pairing, base stacking, and tertiary interactions [9–12]. Furthermore, RNA has special functionalities, such as ribozyme [13], riboswitch [14], siRNA [15], miRNA [16], and RNA aptamers [17], all of which can be seamlessly incorporated into ultrastable RNA nanoparticle scaffolds via sequence fusion for therapeutic intervention in vivo [5, 18–20].

The feasibility of RNA nanotechnology was first demonstrated in 1998 by Peixuan Guo using reengineered pRNA molecules [21] derived from the bacteriophage phi29 DNA packaging motor to form dimer, trimer, and hexamer complexes [22]. The pRNA in its native state forms a hexameric ring to gear one of the most powerful nanomotors known to date. The pRNA monomer has several structural features suitable for constructing multifunctional RNA nanoparticles with defined size, shape, and stoichiometry. In particular, there is an ultrastable three-way junction (3WJ) motif [23, 24] which can be assembled from three short fragments with very high efficiency in the absence of any metal ions. The pRNA-3WJ nanoparticles are homogeneous in size and structure; are thermodynamically [23, 25, 26] and chemically (after 2′-F modifications)

stable [23, 27–29]; are resistant to denaturation in 8 M urea and remain intact at ultralow concentrations [23, 27, 28]; retain authentic folding and independent functionalities of all incorporated modules (RNA aptamer, siRNA, miRNA, or ribozyme) [23, 30]; are nontoxic and biocompatible [31, 32]; are highly soluble; and exhibit favorable biodistribution and pharmacological profiles [23, 27, 28, 31–37]. We have solved the crystal structure [24] of the pRNA-3WJ, thus facilitating the design of multifunctional RNA nanoparticles with tunable size, shape, and stoichiometry.

In construction of nanoparticles, the rigidity of scaffolds is crucial to keep the nanoassemblies well-structured with defined stoichiometry, while the flexibility of angle in each module makes it feasible to form complex structures with controllable sizes and shapes. This unique property of a versatile building block is exemplified by the pRNA-3WJ motif, which adopts an A-type geometry consisting of three helices (H1, H2, and H3) with a planar orientation (Fig. 1A, B). The helices H1 and H3 are coaxially stacked, and form a ~180° angle, while the H1 and H2 helices form a 60° angle

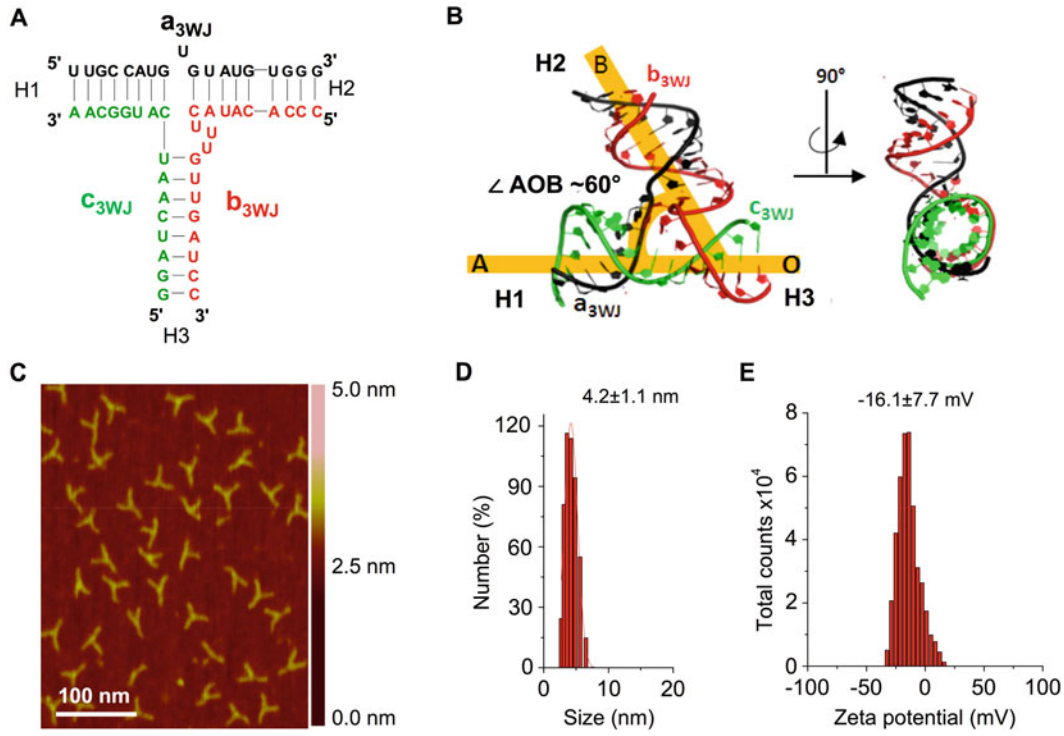

Fig. 1 (**A**) Sequence and (**B**) crystal structure of pRNA-3WJ motif. The 3WJ is composed of three RNA oligomers in *black* (a_{3WJ}), *red* (b_{3WJ}), and *green* (c_{3WJ}). Helical segments are represented as *H1*, *H2*, and *H3*. The internal ∠AOB angle used to construct polygons is shown. (**C**) AFM image of the extended pRNA-3WJ nanoparticles. Dynamic light scattering assay for characterizing the (**D**) size and (**E**) zeta potential of pRNA-3WJ core. Figure reproduced with permission from: (**A**) ref. 23 © Nature Publishing Group; (**B**) ref. 38 © Oxford University Press; (**C**–**E**) ref. 33 © American Chemical Society

[24]. The 3WJ scaffold can be extended to form branched architectures such as X-motif [27] or dendrimer-like 3D globular structures [39] by simple extension of the helical arms. The 3WJ can also serve as a building block to form 2D planar polygonal structures by simply stretching the intrahelical H1-H2 angle to form a triangle ($\angle 60°$), square ($\angle 90°$) and pentagon ($\angle 108°$) pRNA nanoparticles. Each vertex of the polygon contains a 3WJ, which are then linked by double stranded stem regions to form a closed polygon. More recently, we extended the 2D work to design and construct 3D RNA nanoparticles, such as a tetrahedron [37] and prism [40] architectures. Thus, the tunable features of 3WJ structure make it an attractive and unique building unit to construct defined RNA architectures with controllable shapes and sizes.

Physicochemical characteristics of nanoparticles such as size, shape, and surface charge have significant implications in their cellular uptake and in vivo fate after intravenous administration. Generally speaking, nanoparticles with a hydrodynamic diameter of <10 nm are rapidly filtered by the kidneys, while nanoparticles >100 nm are entrapped by the liver Kupffer cells and lung/liver/spleen macrophages. The optimal size range is therefore in the 10–100 nm range to ensure that nanoparticles can enter cells via receptor-mediated endocytosis while avoiding entrapment and rapid excretion. The effect of size and shape on cell entry and trafficking as well as in vivo behavior of nanoparticles is difficult to assess as finding suitable nanoparticles rich in structure while varying in shape and size is challenging. The pRNA-derived nanoparticles with different shape, size, stoichiometry, targeting ligand, and functionalities coupled with their flexibility, versatility, and programmability provide opportunities for these studies. This is exemplified by our recent studies showing that RNA nanoparticles of different size displayed different accumulation in cancer and healthy organs, and RNA nanoparticles with comparable size but different shapes enter different cell types: (1) In cancer xenograft and metastatic mouse models, after systemic injection, pRNA-3WJ nanoparticles accumulated in the tumor microenvironment via EPR (Enhanced Permeability and Retention) effects, strongly bound to tumors and entered the cancer cells via receptor-mediated endocytosis, and was cleared out of vital healthy organs within 8 hours post-administration; (2) Two fluorescent RNA nanoparticles were tested for penetration into ocular tissues through subconjunctival injection into mice [41]. Fluorescent imaging of eye tissue sections revealed that pRNA-3WJ RNA nanoparticles [23] entered the cornea, but not the retina, while the X-shaped pRNA nanoparticles [27] with comparable size as 3WJ, but with different shape entered both the cornea and the retina [41]; (3) In mouse models, triangular shaped RNA nanoparticles with CpG modules have different immunostimulatory effects compared to square and pentagon shaped RNA nanoparticles [38]. These three key findings

indicated that the size and shape of RNA nanoparticles will have a profound impact on targeting of specific cells types. Moreover, the overall negative charge of RNA nanoparticles leads to extensive hydration, and minimizes nonspecific interactions with negatively charged cell membranes and also avoids interactions with serum proteins.

In this chapter, we focus on methods for constructing pRNA nanoparticles of various shapes and sizes using the 3WJ motif as a core scaffold. The physicochemical properties of the RNA nanoparticle can be controlled by the nanoparticle designer from particle inception to completion, due to the bottom-up assembly approach and the numerous toolkits and design strategies that have been developed for RNA nanoparticle construction. These principles are illustrated using the pRNA-3WJ core, pRNA-X motif, 2D square, and 3D tetrahedral RNA nanoparticles. The assembled nanoparticles are then evaluated in cancer and ocular mouse models to demonstrate how the size and shape of RNA nanoparticles influence their biodistribution profiles.

2 Materials

All the reagents must be analytical grade and RNase/DNase free to prevent any nucleic acid degradation. All the solutions and buffers should be prepared using Millipore water (resistivity 18.2 MΩ/cm at 25 °C) treated with diethylpyrocarbonate (DEPC) and then autoclaved. All tubes and glassware used in preparation of buffers and reagents should be autoclaved. Gloves and lab coats should be worn at all times. Prepare and store reagents at room temperature unless otherwise noted.

2.1 Reagents

1. Ammonium persulfate (AP).
2. Tetramethylethylenediamine (TEMED) (*see* **Note 1**).
3. Ethidium bromide (EtBr): 1% Solution, Molecular Grade (*see* **Note 2**).
4. Magnesium chloride hexahydrate ($MgCl_2 \cdot 6H_2O$) (*see* **Note 3**).
5. Urea, for molecular biology, DNase−/RNase−/ and protease-free.
6. Tris–HCl.
7. Sodium chloride (NaCl).
8. Potassium chloride (KCl).
9. Disodium hydrogen phosphate (Na_2HPO_4).
10. Monopotassium phosphate (KH_2PO_4).
11. Ethanol.

12. Boric acid.
13. Bis-acrylamide (*see* **Note 4**).
14. Acrylamide, 99%, electrophoresis grade (*see* **Note 5**).
15. Agarose.
16. Xylene cyanol.
17. Bromophenol blue.
18. Manganese chloride ($MnCl_2$).
19. Spermidine.
20. Dithiothreitol (DTT).
21. Sodium acetate.
22. RNA nucleotide triphosphates (rNTP).
23. Ethylenediaminetetraacetic acid (EDTA).
24. Male/female athymic nude$^{nu/nu}$ (6–8 weeks old) mice, Taconic.
25. Male/female (7–10 weeks old) C57BL/6 mice, Charles River Laboratories.
26. Isoflurane.
27. Buprenorphine.
28. Xylazine.
29. Ketamine.
30. 16% w/v paraformaldehyde solution, Polysciences.
31. Tissue-Tek O.C.T Compound, Andwin Scientific.
32. Hoechst 33342.
33. ProLong Gold Antifade Mountant with DAPI, Life Technologies, Inc.
34. Aqueous mounting medium, Dako.
35. Glass cover slides.
36. Microscope slides.
37. 10% povidone–iodine, Betadine.
38. Phosphoramidites, Glen Research.
39. DNA and RNA Oligo Synthesizer, Azco Biotech.
40. DNA primers, dissolved in water at 100 μM stock concentration, IDT.
41. PCR reaction kit with GoTaq FlexiDNA Polymerase, Promega.
42. Fluorine-modified UTP and CTP at 2′ hydroxyl ribose (2′F-UTP and 2′F-CTP), Trilink.
43. Fetal bovine serum (FBS).

44. Wild type or Y693F mutant T7 RNA polymerase: expressed in-house or acquired commercially, Epibio.
45. MasterCycler Gradient Thermal Cycler Eppendorf 5331, Eppendorf.
46. Typhoon FLA 7000 imaging system, GE Healthcare.
47. Temperature gradient gel electrophoresis (TGGE) system, Biometra.
48. Hand-held Mineralight lamp UVGL-25, UVP.
49. Eppendorf 5424 Centrifuge, Eppendorf.
50. Agarose gel electrophoresis system, mini-sub cell GT system, Bio-Rad.
51. Savant DNA120 SpeedVac concentrator, Thermo Electron Corporation.
52. ISOTEMP 115 Water Bath 15–460-15, Fisher Scientific.
53. NanoDrop 2000 spectrophotometer, Thermo Scientific.
54. Laser scanning confocal microscope, Olympus or Zeis.
55. IVIS spectrum imaging system, PerkinElmer.
56. Atomic force microscope (AFM), Veeco.
57. Dynamic light scattering (DLS), Malvern.
58. High Pressure Liquid Chromatography (HPLC), Agilent.
59. Confocal microscopy, Olympus or Zeis.
60. Alexa Fluor 488 phalloidin (Invitrogen).
61. TO-PRO-3 iodide (642/661) (Invitrogen).
62. Image processing software: Living Image 3.1 software (Caliper Life Sciences) or equivalent.

2.2 Reagent Preparation

1. RNA oligos: Chemically synthesize 2′-F modified RNA oligos (less than 60 nucleotides in length) with or without end-modifications, such as Folate or Alexa 647, using an Oligo synthesizer or custom order from Trilink; Prepare RNA oligos longer than 60 nucleotides by in vitro transcription.
2. DNA primers: Chemically synthesize DNA oligos using an Oligo synthesizer or custom order from *IDT*. Dissolve in DEPC H_2O at desired concentration.
3. DEPC aqueous solution, 0.05% (vol/vol): Add 0.05 ml of DEPC to 99.5 ml water and shake the solution vigorously. Incubate the solution overnight at 37 °C. Autoclave to remove DEPC. This reagent can be stored at room temperature (25 °C) for 1 year.
4. 1× Tris–borate–EDTA (TBE) buffer: 89 mM Tris base, pH 8.0, 86 mM boric acid, and 2 mM EDTA. This buffer can be stored at room temperature for 1 year.

5. 1× Tris–borate–magnesium (TBM) buffer: 89 mM Tris base, pH 8.0, 86 mM boric acid, and 5 mM $MgCl_2$. This buffer can be stored at room temperature for 1 year.
6. 1× Tris–acetate–EDTA (TAE) buffer: 40 mM Tris base, pH 8.0, 20 mM acetic acid, and 1 mM EDTA. This buffer can be stored at room temperature for 1 year.
7. 1× Tris–magnesium–saline (TMS) buffer: 50 mM Tris–HCl (pH 8.0), 100 mM NaCl, and 10 mM $MgCl_2$. Autoclave the solution before use. This buffer can be stored at room temperature for 1 year.
8. Sodium acetate (NaOAc, 3 M, pH 6.5): Autoclave the solution before use. This buffer can be stored at room temperature for 1 year.
9. Magnesium chloride ($MgCl_2 \cdot 6H_2O$, 2 M): This buffer can be stored at room temperature for 1 year.
10. APS: 10% (wt/vol). This reagent can be stored at 4 °C for 1 week.
11. Urea-denaturing PAGE gel, 10–15% (wt/vol): 10–15% (wt/vol; 37.5:1) acrylamide, 8 M urea, 10% (wt/vol) APS and TEMED. The gel needs to be freshly prepared.
12. Native PAGE gel (TBM or TBE): 10–15% (wt/vol): 10–15% (wt/vol; 37.5:1) acrylamide, 1× Tris–borate buffer (pH 7.8), 10 mM $MgCl_2$ (or 2 mM EDTA), 10% (wt/vol) APS and TEMED. The gel needs to be freshly prepared.
13. 1× RNA Elution buffer: 0.5 M ammonium acetate, 10 mM EDTA and 0.1% (wt/vol) SDS in 0.05% (vol/vol) DEPC-treated water. Autoclave the solution before use. This buffer can be stored at room temperature for 6 months.
14. Washing buffer (ethanol 70%): This buffer can be stored at 4 °C for 1 year.
15. 6× Native gel loading buffer: 40% (wt/vol) sucrose, 0.1% (wt/vol) xylene cyanol, and 0.1% (wt/vol) bromophenol blue. This buffer can be stored at −20 °C for 1 year.
16. 1× PBS buffer: 137 mM NaCl, 2.7 mM KCl, 10 mM Na_2HPO_4, and 2 mM KH_2PO_4 (pH 7.4). Autoclave the solution before use. This buffer can be stored at room temperature for 1 year.
17. Tissue fixation buffer: 4% Paraformaldehyde and 10% sucrose in 1× PBS buffer. Use immediately or store at 4 °C up to 1 week.
18. RNA nucleotide triphosphates (rNTP) 100 mM, adjust pH to 7.5 with NaOH. This reagent can be stored at −20 °C for 1 year.

19. 1× 2′-F transcription buffer: 40 mM Tris–acetate, pH 8.0, 0.5 mM DTT, 1 mM EDTA, 10 mM $Mg(OAc)_2$, 0.5 mM $MnCl_2$, 16 mM spermidine. This buffer can be stored at −20 °C for 1 year.
20. 1× T7 RNA polymerase transcription buffer: 40 mM HEPES–KOH, pH 7.5, 24 mM $MgCl_2$, 2 mM spermidine, 2 mM, 40 mM DTT. This buffer can be stored at −20 °C for 1 year.

3 Methods

General procedures such as PCR amplification, in vitro RNA transcription, solid-phase RNA synthesis, and RNA nanoparticle assembly have been discussed in detail previously [42–46].

3.1 Assembly of pRNA-3WJ Core

The 3WJ core is composed of three short strands a_{3wj}, b_{3wj}, and c_{3wj} (Fig. 1A, B). The three helical branches are denoted H1, H2, and H3, respectively. The 3WJ serves as the core scaffold for constructing RNA squares and RNA tetrahedrons outlined here.

1. Chemically synthesize three RNA oligo components of the pRNA-3WJ: a_{3wj}, b_{3wj}, and c_{3wj}.
2. Mix the three strands in equimolar ratio in DEPC-treated water or TBE/TMS buffer. No metal ions (such as NaCl or $MgCl_2$) or annealing procedure (heating to 95 °C and slowly cooling to room temperature) is necessary since the assembly occurs almost spontaneously in water.
3. Load the assembled complex(3WJ-a/b/c) and control strands (a_{3wj}, b_{3wj}, c_{3wj}, a_{3wj}/b_{3wj}, b_{3wj}/c_{3wj}, a_{3wj}/c_{3wj}) onto an 15% (wt/vol) native PAGE gel and run the gel in TBM or TBE buffer at 100 V and 4 °C for around 2 h. Visualize the RNA by ethidium bromide staining using Typhoon FLA 7000. Since the 3WJ assembles with high efficiency, only one band should be observed and it will run slightly ahead of xylene cyanol.
4. Characterize the structure of 3WJ complex by atomic force microscope (*see* **Note 6**) (Fig. 1C); and dynamic light scattering (*see* **Note 7**) for measuring the hydrodynamic size and zeta potential (Fig. 1D, E).

3.2 Assembly of pRNA-3WJ with Functionalities and Extension to Form pRNA-X Scaffold

Folate or RNA aptamer can be used as targeting ligand; Alexa 647 or other fluorophores, especially near infrared dyes, can be used as imaging module.

1. Chemically synthesize three RNA oligo components of the pRNA-3WJ-Folate-Alexa647 nanoparticle with end-modifications: a_{3wj}-Folate, b_{3wj}, and c_{3wj}-Alexa 647.

2. Mix the three strands in equimolar ratio in DEPC-treated water or TBE/TMS buffer at room temperature.
3. Load the assembled complex and control strands onto an 15% (wt/vol) native PAGE gel and run the gel in TBM or TBE buffer at 100 V and 4 °C for around 2 h. Visualize the RNA by ethidium bromide staining or Alexa 647 fluorescence using Typhoon FLA 7000. If necessary, purify the complex from the gel and elute the RNA using the elution buffer for 4 h at 37 °C, followed by ethanol precipitation overnight.
4. Characterize the structure of the 3WJ complex by atomic force microscope (*see* **Note 6**); and dynamic light scattering (*see* **Note 7**) for measuring the hydrodynamic size and zeta potential.
5. The X-shaped motif builds on the 3WJ core by branch extension and consists of four strands, denoted a, b, c, and d (Fig. 2A). The four helical regions are denoted H1, H2, H3,

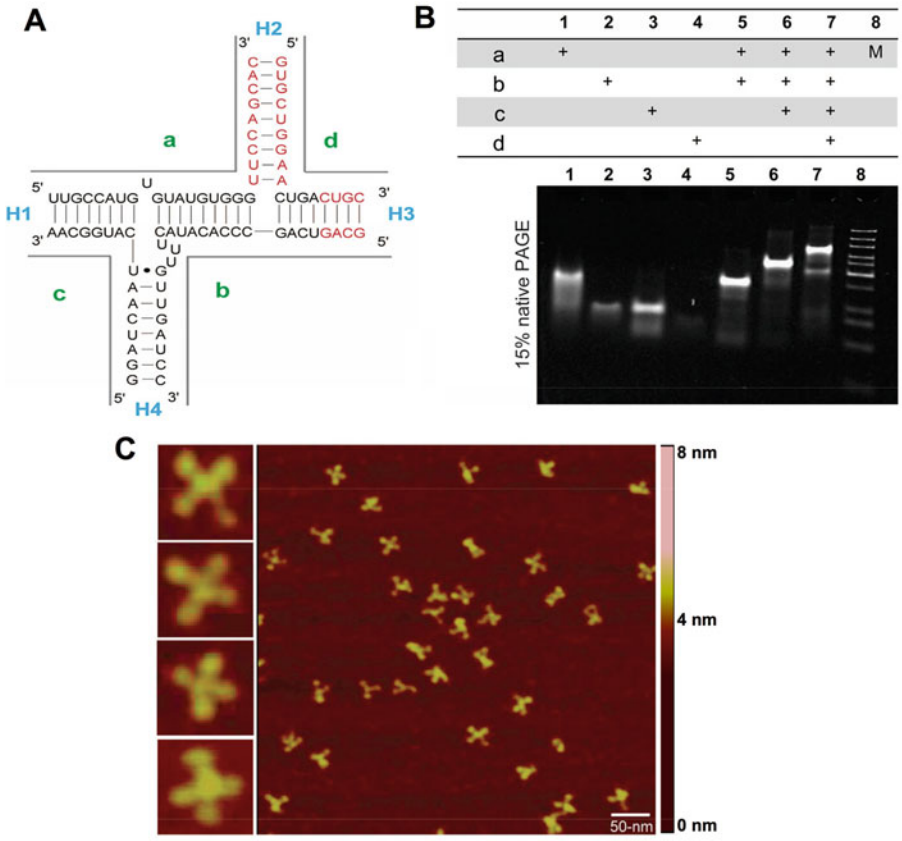

Fig. 2 (**A**) Sequence of pRNA-X motif. The nucleotides in *red* indicate new sequences that were added to the original pRNA sequences in *black* [27]. The core is composed of four RNA oligos (denoted *a*, *b*, *c*, and *d*). Helical segments are represented as *H1*, *H2*, *H3*, and *H4*. (**B**) 15% native PAGE showing the stepwise assembly of the pRNA-X core from component strands. In the table '+' indicates the presence of the strand in the complex. (**C**) AFM images of pRNA-X constructs harboring four pRNA monomer units at the branch ends. Figure reproduced with permission from ref. 27 © Elsevier

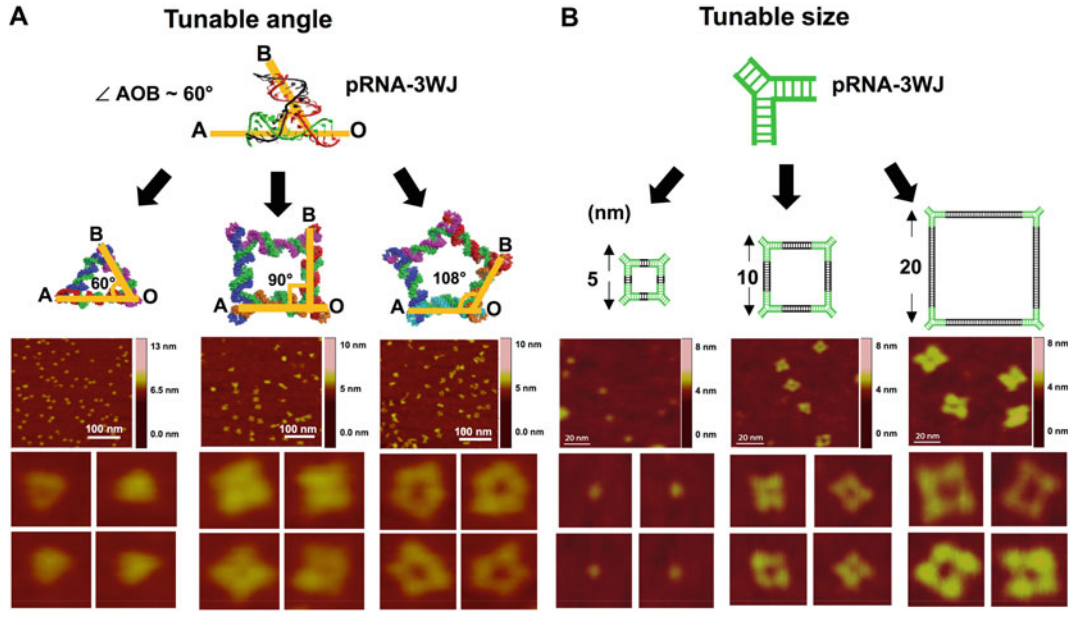

Fig. 3 Design and characterization of RNA nanoparticles with tunable shape and size. (**A**) AFM images of *triangle* (∠AOB 60°), *square* (∠AOB 90°) and *pentagon* (∠AOB 108°) nanoparticles derived from the pRNA-3WJ motif. (**B**) AFM images of small (5 nm), medium (10 nm), and large (20 nm) RNA squares derived from pRNA-3WJ. Figure reproduced with permission from: (**A**) ref. 38 © Oxford University Press; (**B**) ref. 48 © American Chemical Society

and H4. Synthesize the strands chemically and then proceed with the assembly (Fig. 2B), purification, and characterization (Fig. 2C) steps outlined in **steps 1–4** above.

3.3 Construction of 2D Planar RNA Squares with Same Shape but Variable Size Using 3WJ as Modules

Previously it has been shown that the intrahelical H1–H2 angle of 3WJ can be stretched to form 2D planar triangle (∠60°), square (∠90°) and pentagon (∠108°) pRNA nanoparticles [38, 47] (Fig. 3a). Herein, the RNA square [48] is used as an example for constructing RNA nanoparticles of various sizes (Fig. 3b).

1. Design RNA nanosquares using the Swiss PDB viewer. Open four copies of the pRNA-3WJ crystal structure (PDB ID: 4KZ2) and four copies of 8 bp RNA duplex, which will act as a connecting duplex between H1 and H2 of each 3WJ. Align each 3WJ in a planar fashion in square configuration and insert RNA duplex in-between H1 and H2 of each pRNA-3WJ.
2. Extend each corner of the square, H3 of the 3WJ, by five base pairs to increase thermodynamic stability and strand diversity (*see* **Note 8**). To construct the square, use a total of five strands: Four short strands (42 nt) that make up each edge of the square, and one long strand (88 nt) that makes up the middle core strand, connecting each of the strands. In this form, the edges are about 10 nm in length from arm to arm.

3. To construct different size of RNA squares, simply decrease or increase the number of base pairs that connect each 3WJ at the vertices. To make a small square decrease each edge by 11 bp in length. This will result in external strands of 31 nt in length and an internal strand with length of 44 nt. The resulting square will be about 5 nm in length from arm to arm on each edge. Conversely, to design a square of about 20 nm along each edge, increase each edge by 22 nt, two turns of RNA duplex. This results in external strands of 66 nt in length and an internal strand with a length of 176 nt (*see* **Note 9**).
4. Synthesize the designed RNA strands chemically if the strands are <60 nt. For longer strands, use in vitro transcription. Prepare the DNA templates including the T7 RNA polymerase promoter region (sequence: 5′-TAA TAC GAC TCA CTA TA-3′) by PCR (*see* **Note 10**). Purify the strands by HPLC or denaturing PAGE.
5. Assemble the RNA squares by annealing (heating at 95 °C for 5 min followed by slow cooling to 4 °C) the five strands in equimolar ratio in 1× TMS buffer.
6. Perform a stepwise assembly process (as in Fig. 2B) to determine the migration rate of the final square construct. Mix one additional strand for each sample and load onto an 8% native PAGE gel. Run the gel for 100 min at 100 V constant current at 4 °C in TBM buffer to preserve native conditions. Use total RNA staining with ethidium bromide to visualize RNA bands. Observe a decrease in migration rate going from monomer to dimer, to trimer, to tetramer, and finally to square nanoparticle. Characterize the RNA squares of different sizes using AFM imaging (Fig. 3) and DLS (as in Fig. 2D, E).

3.4 Construction of pRNA-3WJ Based 3D RNA Tetrahedrons of Different Sizes

1. Design the RNA tetrahedrons using UCSF Chimera and Swiss PDB viewer. Open the PDB file of the pRNA-3WJ motif (PDB ID: 4KZ2). Since the 3D conformation of the pRNA-3WJ motif is flexible, use UCSF Chimera to manually change the angles among the three-branched RNA double helices in order to fit the structure into the corners of the designed RNA tetrahedron. Then use Swiss PDB Viewer to align four pRNA-3WJ motifs and six RNA double helices to construct the computational model of the designed RNA tetrahedron. In the final form, the RNA tetrahedron will be composed of a total of four strands with a pRNA-3WJ motif positioned in the corners and RNA double helices positioned along the edges of the tetrahedron (Fig. 4A). Optimize the sequences using *mfold* [49] (*see* **Note 9**). For incorporating targeting ligands, such as RNA aptamer, simply incorporate the sequences at the 3′-end of the core strands, as illustrated with EGFR targeting RNA aptamers [37] (Fig. 4B).

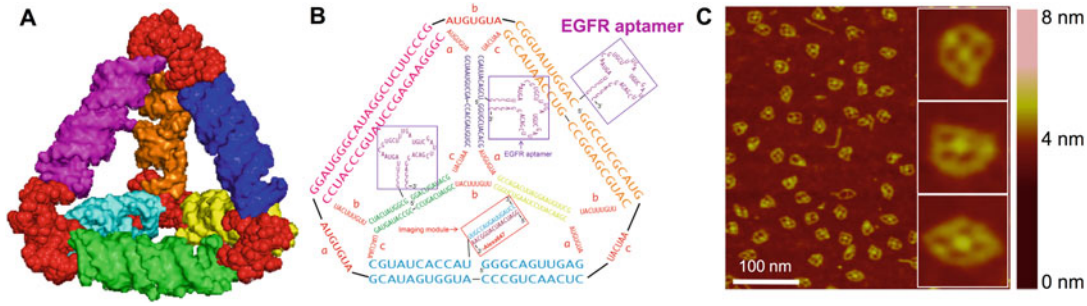

Fig. 4 (**A**) 3D computational model of RNA tetrahedrons. (**B**) Sequence of RNA tetrahedrons harboring imaging module and EGFR targeting RNA aptamers. (**C**) AFM imaging of RNA tetrahedrons. Figure reproduced with permission from ref. 37 © John Wiley & Sons, Inc.

2. For designing smaller or larger RNA tetrahedrons, simply decrease or increase every edge of the tetrahedron by 11 bp (one helical turn), respectively.
3. After finalizing the designs, synthesize the four RNA strands by in vitro transcription. Prepare the DNA templates including the T7 RNA polymerase promoter region by PCR. Purify the strands by 8 M urea, 8% denaturing PAGE.
4. For generating RNA tetrahedrons resistant to serum degradation, during transcription, use Y693F mutant T7 polymerase and 2′-F modified cytosine (C) and uracil (U) nucleotides in the sequence.
5. Assemble the RNA tetrahedrons by mixing the four strands in equimolar concentrations in 1× Tris buffer (100 mM NaCl, 50 mM Tris, pH 8.0), and heated to 95 °C for 5 min and slowly cooled to 4 °C over 45 min by using a thermal cycler.
6. Observe the stepwise assembly of the RNA tetrahedrons by running the RNA tetrahedrons and assemble intermediates in native PAGE gels run in 1× TBM buffer at 90 V, 4 °C. Visualize the RNA after ethidium bromide staining by Typhoon FLA 7000.
7. Characterize the RNA tetrahedrons of different sizes using AFM imaging (Fig. 4C) and DLS assay.

3.5 In Vitro Cell Binding and Internalization of pRNA-3WJ Based Nanoparticles Assayed by Confocal Microscopy

1. For assaying folate-labeled RNA nanoparticles, use folate receptor positive cells, such as KB cells. Maintain the cells in complete culture medium (RPMI-1640 with 10% fetal bovine serum).
2. One day before the binding study, trypsinize the cells using 0.25% Trypsin-EDTA and seed 1 × 10^5 cells in 24-well plate with clean glass cover slide in each well using RPMI-1640 complete culture medium containing no folate (*see* **Note 11**).

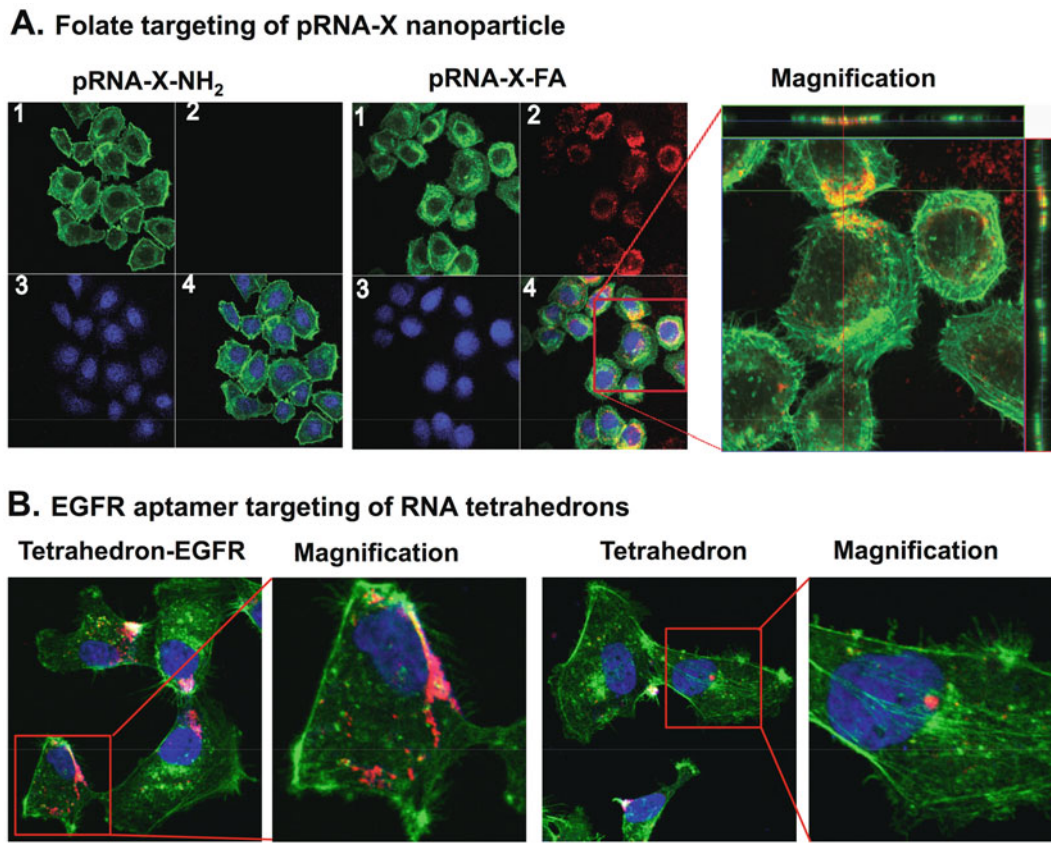

Fig. 5 Confocal microscopy images showing targeting of (**A**) pRNA-X nanoparticles harboring folate (or amine as control) to folate receptor positive KB cells and (**B**) RNA tetrahedrons (with and without EGFR aptamers) to MDA-MB-231 cells. In the images, nucleus (*blue*), cytoplasm (*green*), and RNA nanoparticles (*red*) are shown. In (**B**), only the overlapped images are shown. Figure reproduced with permission from: (**A**) ref. 27 © Elsevier; (**B**) ref. 37 © John Wiley & Sons, Inc.

3. Once the cell attaches to the glass slide, rinse the cells with blank RPMI-1640 medium containing no folate.
4. Incubate cells with 200–400 nM of pRNA-X-Folate-Alexa647 RNA nanoparticles (or with control RNA nanoparticles without folate) at 37 °C for 1–4 h. Similar assays can be done using pRNA-3WJ-Folate-Alexa647 nanoparticles.
5. After washing with PBS, fix the cells with 4% paraformaldehyde and stain by Alexa Fluor 488 phalloidin for the cytoskeleton and TO-PRO-3 iodide (642/661) for the nucleus. Assess cell binding and internalization with a laser scanning confocal microscope (Fig. 5A).
6. For assaying the EGFR aptamer mediated targeting in vitro, grow EGFR-positive cells, such as MDA-MB-231 cells on glass cover slides in 24-well plates in DME–F-12 (1:1) medium with 10% FBS at 37 °C in humidified air containing 5% CO_2

overnight. Dilute RNA tetrahedrons harboring EGFR aptamers (or controls) in Opti-MEM medium to 100 nM and incubate with the cells for 1 h at 37 °C. Once the cell attaches to the glass slide, rinse the cells with blank Opti-MEM medium and conduct step [5] (Fig. 5b).

3.6 Biodistribution Assessment of pRNA-3WJ, pRNA-X, and RNA Tetrahedral Nanoparticles in Cancer Xenograft Mouse Models After Systemic Injection

1. Obtain male/female athymic nude$^{nu/nu}$ (6–8 weeks old) mice. Keep the mice in clean, pathogen-free rooms in an environment with controlled temperature (27 °C), humidity, and a 12 h. light–dark cycle. Feed the mice with a folate-free diet (Harlan Laboratories; Indianapolis, IN) for at least 2 weeks before the experiment. Make sure that a proper protocol regarding animal experiments is in place at the institution to conduct the animal studies.
2. Inject the mouse subcutaneously with KB cells (3×10^6 cells in 100 μl PBS). Pinch the skin of the mouse with forceps and pull the skin away from the body of the mouse. Inject slowly and evenly into the pouch created by pulling the skin. Try to create a single bubble of cells beneath the skin (*see* **Note 12**). Gently remove the needle and hold the injection site with forceps for 10 s to prevent retrograde cell suspension flow.
3. Monitor the tumor growth for a few weeks using calipers until the tumors are about 500 mm^3.
4. Anesthetize the mice using isoflurane gas (2% in oxygen at 0.6 L/min flow rate).
5. Intravenously inject through the tail vein with a single dose of 3 μg 2′-F U/C modified pRNA-3WJ-Folate-Alexa647 (or pRNA-X-Folate-Alexa647) per g of mouse body weight in 300 μL of PBS.
6. Conduct whole-body imaging (excitation: 650 nm; emission: 668 nm) at 1, 4 and 8 h after RNA nanoparticle administration on an IVIS Spectrum station (Fig. 6a, b).
7. Obtain composite images comprising of black and white digital photos with an overlay of images reflecting fluorescent activity. Generate a density map (photons/second/cm^2/steradian; p/s/cm^2/sr) using the image processing software and represent it as a color gradient centered at the maximal spot.
8. Following CO_2 asphyxiation at 8 h time point, remove the tumor, liver, heart, lung and kidney of the mice for ex vivo imaging of the organs (Fig. 6A, B).
9. To generate orthotopic Triple Negative Breast Cancer xenograft tumors, inject 2×10^6 MDA-MB-231 cells suspended in PBS directly into the mammary fat pad of the mice. Typically, the xenograft tumors will be apparent within 2 weeks after the implantation. Follow **steps 4–8** to assay RNA tetrahedrons harboring EGFR targeting aptamers (Fig. 6C).

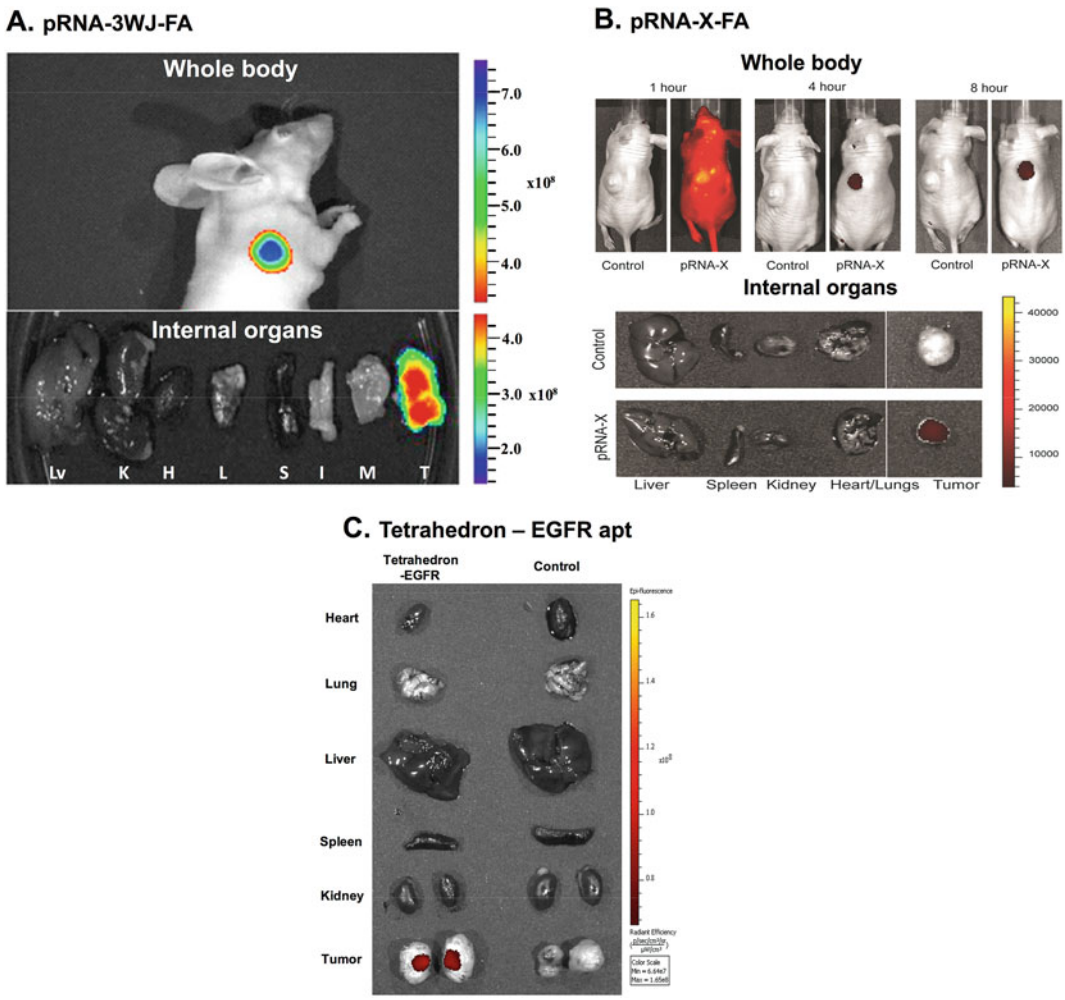

Fig. 6 Biodistribution assay showing targeting of (**A**) pRNA-3WJ-Folate-Alexa647 and (**B**) pRNA-X-Folate-Alexa647 nanoparticle to Folate receptor(+) subcutaneous tumor xenografts after systemic injection in nude mice. *Upper panel*: whole body; *lower panel*: organ imaging (*Lv* liver, *K* kidney, *H* heart, *L* lung, *S* spleen, *I* intestine, *M* muscle, *T* tumor). (**C**) Internal organ images showing the targeting of RNA tetrahedrons harboring EGFR aptamers to orthotopic MDA-MB-231 breast tumors after tail vein injection. Figure reproduced with permission from: (**A**) ref. 23 © Nature Publishing Group; (**B**) ref. 27 © Elsevier; (**C**) ref. 37 © John Wiley & Sons, Inc.

3.7 Assessment of Ocular Biodistribution of pRNA-3WJ Based Nanoparticles After Subconjunctival Injection in Mouse Models

1. Obtain 7–10 weeks old C57BL/6 male/female mice. Keep the mice in clean, pathogen-free rooms in an environment with controlled temperature (27 °C), humidity, and a 12 h light–dark cycle.
2. Anesthetize the mouse by intraperitoneal injection of 10 mg/kg xylazine and 80 mg/kg ketamine.
3. Gently pull the conjunctiva from the sclera with a pair of forceps. Inject 10 μL of pRNA-3WJ, pRNA-X, dsRNA, or

Alexa 647 dye into the superior subconjunctival region using a microsyringe with a 33 G needle.

4. Perform whole-body fluorescence imaging after subconjunctival injection (*see* **Note 13**) (Fig. 7A). Keep the mice anesthetized with 2% isoflurane during the imaging. Use the following imaging parameters: 630 nm (excitation) and 700 nm (emission), field of view (FOV) of 120 mm, f-stop of 2.51, 4 × 4 pixel binning, and exposure time of 1 s. For higher resolution, use the same parameters except with FOV of 22 mm, 1 × 1 pixel binning, and exposure time of 5 s.
5. For anatomical reference, perform X-ray (exposure time of 30 s) and surface optical imaging (exposure time of 0.175 s) with the same FOV as the fluorescence imaging.
6. To monitor ocular clearance of the pRNA-3WJ, pRNA-X nanoparticles, dsRNA (control), and Alexa 647 (dye only as control), perform fluorescence imaging at predetermined time points (e.g., 0.5, 1, 2, 4, 6, 7.5, and 9.5 h) after the injection. After each imaging scan, return the mice to their cages.
7. Overlay the fluorescence images with the corresponding anatomical reference images and manually select region of interest (ROI) to calculate the mean fluorescence intensities of the ROI at different time points.
8. Sacrifice the mice by cervical dislocation under anesthesia at predetermined time points (e.g., 6, 12, and 20 h after subconjunctival injection) (Fig. 7B–F). Collect the eyes including the conjunctiva and eyelids and wash them with PBS for 2 × 30 min at room temperature to remove blood and other contaminations. Fix the eyes on a piece of wax in 4% paraformaldehyde solution for 2 h at 4 °C to ensure that the conjunctivas are flattened.
9. Dissect the eyes and isolate tissues of conjunctiva, cornea, retina, and sclera. Stain with 0.01% DAPI solution overnight at room temperature. Rinse the tissues with PBS for 3 × 10 min and mount on a glass slide with Mowoil (PVA) for fluorescence imaging.
10. Image the tissues using wavelength of 461 nm for the cell nucleus stained by DAPI and 665 nm for the Alexa 647 marker. Analyze the images by counting the numbers of cells with the cell nucleus surrounded by or overlapped with Alexa647 signals (for assessing cell internalization) in 0.42 mm × 0.33 mm FOV at the same imaging plane in the tissues (Fig. 7B–F).

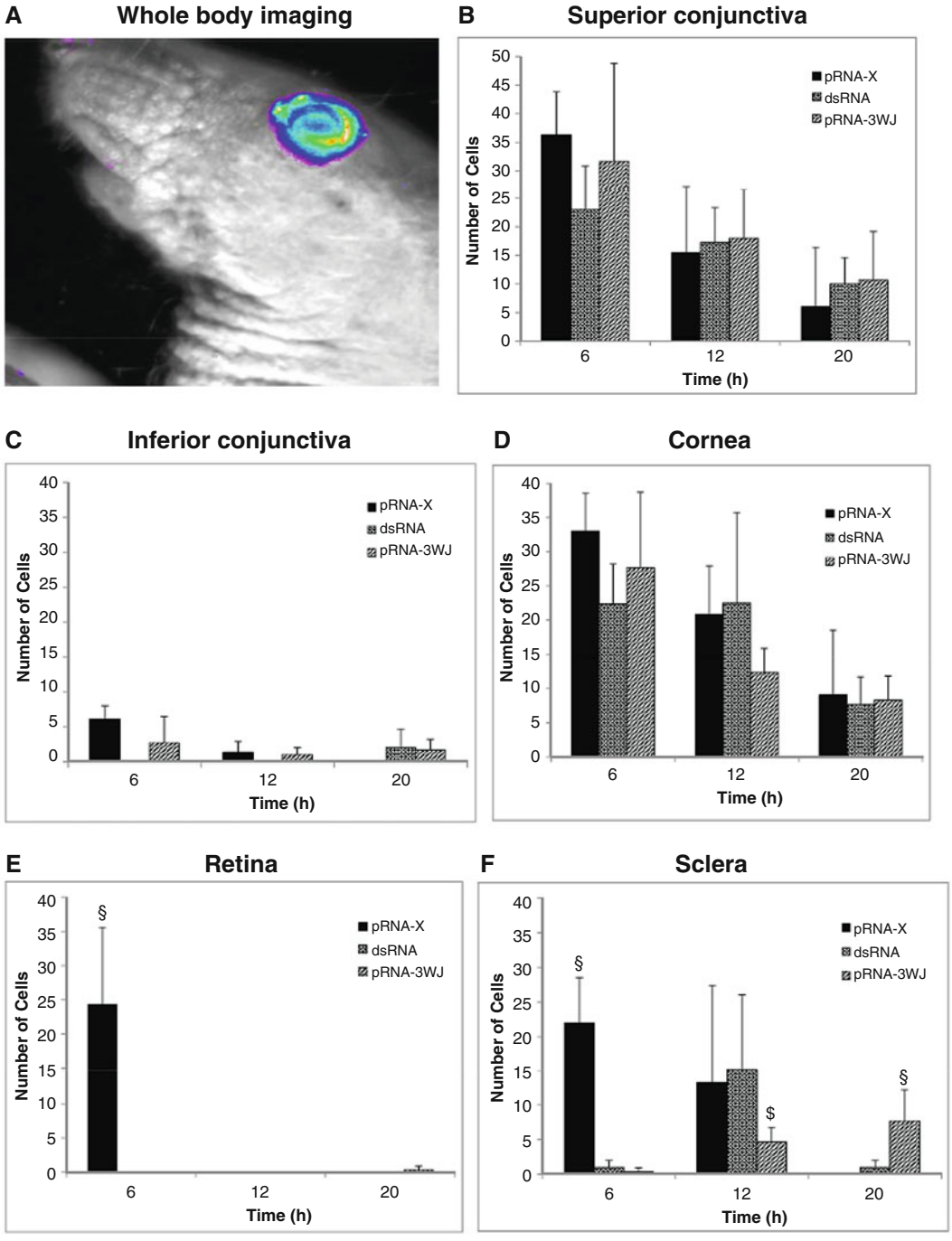

Fig. 7 Assessment of ocular delivery of pRNA nanoparticles in mouse models. (**A**) Whole body imaging of the eye after subconjunctival injection of pRNA nanoparticle (2 h time point). (**B–F**) Numbers of cells with pRNA-3WJ, pRNA-X, and dsRNA (control) internalization in different cells after subconjunctival injection: (**B**) superior conjunctiva (near the injection site); (**C**) inferior conjunctiva; (**D**) cornea; (**E**) retina; (**F**) sclera. Figure reproduced with permission from ref. 41 © Springer

4 Notes

1. TEMED is a skin and respiratory tract irritant.
2. Ethidium bromide is mutagenic and moderately toxic, and must be handled with care. It is a strong carcinogen and is a skin, eye, and respiratory tract irritant. Wear gloves while dispensing it in a hood.
3. $MgCl_2$ will absorb moisture from the air. Be sure to handle as quickly as possible and then recap the reagent bottle tightly to prevent moisture absorption.
4. Bis-acrylamide causes eye, skin, and respiratory tract irritation. It is harmful if inhaled, swallowed or absorbed through skin. It may cause CNS effects. Wear gloves, goggles, and a mask when you are handling it.
5. Acrylamide may cause cancer and heritable genetic damages. It is harmful on inhalation and on contact with skin. It is toxic if swallowed. Wear gloves and a mask when you are handling it.
6. Due to the resolution limit of AFM imaging affected by the probe size of 4–10 nm, pRNA-3WJ and pRNA-X nanoparticles are too small to be reliably imaged with detailed structure and shape. To evaluate the global structures of the RNA nanoparticles derived from the 3WJ core, dsRNA is appended to the three arms of the 3WJ core (Fig. 1C). Similarly, for pRNA-X core, four pRNA monomers are incorporated for AFM imaging (Fig. 2C).
7. It is important to note that RNA nanoparticles are not globular in shape, and deviations from DLS measurements are expected, since the hydrodynamic size from DLS corresponds to the average of the three dimensions of RNA nanoparticles due to rapid tumbling in solution.
8. When choosing the nucleotide sequence for the 8 base pair connecting helix and 5 base pair extension sequences, it is important to introduce sequence diversity while also avoiding nonspecific base interactions into the structure. Optimize the sequences using the *mfold* RNA folding software [49].
9. To maintain planar geometry, it is important to decrease or increase each edge in multiples of 11 bp, as one complete turn of RNA duplex is equal to 11 bp.
10. Adding two guanosine nucleotides to the DNA template sequence immediately following the T7 promoter typically enhances the RNA transcription efficiency.
11. To ensure sufficient binding, the cells need to be kept in a folate-free medium for at least 12 h before the binding assay.

12. Try to avoid too much spreading of the cells. In addition, prepare large amount of cells to avoid inevitable loss during the experimental handling process.
13. Keep the ocular surface and surrounding area clean with saline before the first imaging to ensure that there is no significant contamination from the residues from the dosing.

Acknowledgments

The research was supported by NIH grants R01EB019036, U01CA151648 and U01CA207946. P.G.'s Sylvan G. Frank Endowed Chair position in Pharmaceutics and Drug Delivery is funded by the CM Chen Foundation. P.G. is the founder of P&Z Biological Technology and a consultant of Oxford Nanopore and Nanobiodelivery Pharmaceutical Co. Ltd.

References

1. Puri A, Loomis K, Smith B et al (2009) Lipid-based nanoparticles as pharmaceutical drug carriers: from concepts to clinic. Crit Rev Ther Drug Carrier Syst 26:523–580
2. Weijun L, Francis CS (2007) Lipid-based nanoparticles for nucleic acid delivery. Pharm Res 24:438–449
3. Vo-Dinh T (2005) Protein nanotechnology: the new frontier in biosciences. Methods Mol Biol 300:1–13
4. Zhang F, Nangreave J, Liu Y et al (2014) Structural DNA nanotechnology: state of the art and future perspective. J Am Chem Soc 136:11198–11211
5. Guo P (2010) The emerging field of RNA nanotechnology. Nat Nanotechnol 5:833–842
6. Seeman NC (1982) Nucleic acid junctions and lattices. J Theor Biol 99:237–247
7. Seeman NC (2010) Nanomaterials based on DNA. Annu Rev Biochem 79:65–87
8. Lin C, Liu Y, Yan H (2009) Designer DNA nanoarchitectures. Biochemistry 48:1663–1674
9. Sugimoto N, Nakano S, Katoh M et al (1995) Thermodynamic parameters to predict stability of RNA/DNA hybrid duplexes. Biochemistry 34:11211–11216
10. Searle MS, Williams DH (1993) On the stability of nucleic acid structures in solution: enthalpy-entropy compensations, internal rotations and reversibility. Nucleic Acids Res 21:2051–2056
11. Lemieux S, Major F (2002) RNA canonical and non-canonical base pairing types: a recognition method and complete repertoire. Nucleic Acids Res 30:4250–4263
12. Leontis NB, Westhof E (2001) Geometric nomenclature and classification of RNA base pairs. RNA 7:499–512
13. Scott WG (2007) Ribozymes. Curr Opin Struct Biol 17:280–286
14. Breaker RR (2012) Riboswitches and the RNA world. Cold Spring Harb Perspect Biol 4: a003566
15. Ryther RC, Flynt AS, Phillips JA III et al (2005) siRNA therapeutics: big potential from small RNAs. Gene Ther 12:5–11
16. Ha M, Kim VN (2014) Regulation of microRNA biogenesis. Nat Rev Mol Cell Biol 15:509–524
17. Zhou J, Bobbin ML, Burnett JC et al (2012) Current progress of RNA aptamer-based therapeutics. Front Genet 3:234
18. Shu Y, Pi F, Sharma A et al (2014) Stable RNA nanoparticles as potential new generation drugs for cancer therapy. Adv Drug Deliv Rev 66C:74–89
19. Guo P, Haque F, Hallahan B et al (2012) Uniqueness, advantages, challenges, solutions, and perspectives in therapeutics applying RNA nanotechnology. Nucleic Acid Ther 22:226–245

20. Li H, Lee T, Dziubla T et al (2015) RNA as a stable polymer to build controllable and defined nanostructures for material and biomedical applications. Nano Today 10:631–655
21. Guo P, Erickson S, Anderson D (1987) A small viral RNA is required for *in vitro* packaging of bacteriophage phi29 DNA. Science 236: 690–694
22. Guo P, Zhang C, Chen C et al (1998) Inter-RNA interaction of phage phi29 pRNA to form a hexameric complex for viral DNA transportation. Mol Cell 2:149–155
23. Shu D, Shu Y, Haque F et al (2011) Thermodynamically stable RNA three-way junctions for constructing multifuntional nanoparticles for delivery of therapeutics. Nat Nanotechnol 6:658–667
24. Zhang H, Endrizzi JA, Shu Y et al (2013) Crystal structure of 3WJ core revealing divalent ion-promoted thermostability and assembly of the Phi29 hexameric motor pRNA. RNA 19:1226–1237
25. Binzel DW, Khisamutdinov EF, Guo P (2014) Entropy-driven one-step formation of Phi29 pRNA 3WJ from three RNA fragments. Biochemistry 53:2221–2231
26. Binzel D, Khisamutdinov EF, Vieweger M et al (2016) Mechanism of three-component collision to produce ultra-stable pRNA three-way junction of Phi29 DNA-packaging motor by kinetic assessment. RNA 22:1710–1718
27. Haque F, Shu D, Shu Y et al (2012) Ultrastable synergistic tetravalent RNA nanoparticles for targeting to cancers. Nano Today 7:245–257
28. Shu Y, Haque F, Shu D et al (2013) Fabrication of 14 different RNA nanoparticles for specific tumor targeting without accumulation in normal organs. RNA 19:766–777
29. Liu J, Guo S, Cinier M et al (2011) Fabrication of stable and RNase-resistant RNA nanoparticles active in gearing the nanomotors for viral DNA packaging. ACS Nano 5:237–246
30. Shu D, Khisamutdinov E, Zhang L et al (2013) Programmable folding of fusion RNA complex driven by the 3WJ motif of phi29 motor pRNA. Nucleic Acids Res 42:e10
31. Abdelmawla S, Guo S, Zhang L et al (2011) Pharmacological characterization of chemically synthesized monomeric pRNA nanoparticles for systemic delivery. Mol Ther 19:1312–1322
32. Cui D, Zhang C, Liu B et al (2015) Regression of gastric cancer by systemic injection of RNA nanoparticles carrying both ligand and siRNA. Sci Rep 5:10726
33. Shu D, Li H, Shu Y et al (2015) Systemic delivery of anti-miRNA for suppression of triple negative breast cancer utilizing RNA nanotechnology. ACS Nano 9:9731–9740
34. Binzel D, Shu Y, Li H et al (2016) Specific delivery of MiRNA for high efficient inhibition of prostate cancer by RNA nanotechnology. Mol Ther 24(7):1267–1277
35. Rychahou P, Haque F, Shu Y et al (2015) Delivery of RNA nanoparticles into colorectal cancer metastases following systemic administration. ACS Nano 9:1108–1116
36. Lee TJ, Haque F, Shu D et al (2015) RNA nanoparticles as a vector for targeted siRNA delivery into glioblastoma mouse model. Oncotarget 6:14766–14776
37. Li H, Zhang K, Pi F et al (2016) Controllable self-assembly of RNA tetrahedrons with precise shape and size for cancer targeting. Adv Mater 34:7501–7507
38. Khisamutdinov E, Li H, Jasinski D et al (2014) Enhancing immunomodulation on innate immunity by shape transition among RNA triangle, square, and pentagon nanovehicles. Nucleic Acids Res 42:9996–10004
39. Sharma A, Haque F, Pi F et al (2015) Controllable self-assembly of RNA dendrimers. Nanomed Nanotechnol Biol Med 12:835–844
40. Khisamutdinov EF, Jasinski DL, Li H et al (2016) Fabrication of RNA 3D nanoprism for loading and protection of small RNAs and model drugs. Adv Mater 28(45): 10079–10087
41. Feng L, Li SK, Liu H et al (2014) Ocular delivery of pRNA nanoparticles: distribution and clearance after subconjunctival injection. Pharm Res 31:1046–1058
42. Shu Y, Shu D, Haque F et al (2013) Fabrication of pRNA nanoparticles to deliver therapeutic RNAs and bioactive compounds into tumor cells. Nat Protoc 8:1635–1659
43. Rychahou P, Shu Y, Haque F et al (2015) Methods and assays for specific targeting and delivery of RNA nanoparticles to cancer metastases. Methods Mol Biol 1297:121–135
44. Lee TJ, Haque F, Vieweger M et al (2015) Functional assays for specific targeting and delivery of RNA nanoparticles to brain tumor. Methods Mol Biol 1297:137–152
45. Jasinski D, Schwartz C, Haque F et al (2015) Large scale purification of RNA nanoparticles by preparative ultracentrifugation. Methods Mol Biol 1297:67–82

46. Zhang H, Pi F, Shu D et al (2015) Using RNA nanoparticles with thermostable motifs and fluorogenic modules for real-time detection of RNA folding and turnover in prokaryotic and eukaryotic cells. Methods Mol Biol 1297: 95–111
47. Khisamutdinov EF, Bui MN, Jasinski D et al (2015) Simple method for constructing RNA triangle, square, Pentagon by tuning interior RNA 3WJ angle from 60 degrees to 90 degrees or 108 degrees. Methods Mol Biol 1316: 181–193
48. Jasinski D, Khisamutdinov EF, Lyubchenko YL et al (2014) Physicochemically tunable poly-functionalized RNA square architecture with fluorogenic and ribozymatic properties. ACS Nano 8:7620–7629
49. Zuker M (2003) Mfold web server for nucleic acid folding and hybridization prediction. Nucleic Acids Res 31:3406–3415